RSC Advances

ROYAL SOCIETY OF CHEMISTRY

www.rsc.org/advances

Study on the reaction mechanism and kinetic of CO hydrogenation on the fused Fe-Mn catalyst

A. A. Mirzaei[1], E. Rezazadeh[1], M. Arsalanfar[2*], M. Abdouss[2], M. Fatemi[1], M. Sahebi[1]

1. Department of chemistry, Faculty of sciences, University of Sistan and Baluchestan, P.O. Box 98135-674, Zahedan, Iran.

Tel: +98 (541) 2447231, Fax: +98 (541) 2447231

2. Department of chemistry, Amirkabir University of technology, Hafez Ave, Tehran, Iran

* corresponding author **Email: maryam_galavy@yahoo.com**

Abstract

The kinetic of CO hydrogenation reaction over the Fe–Mn fused catalyst was investigated in a fixed bed micro-reactor under following conditions: temperature of 573–603 K, pressure of 1–15 bar, H_2/CO feed ratio of 0.7–3.4 and space velocity of 4500 h^{-1}. Reaction rate equation for supported Fe-Mn catalyst was derived on the basis of the Langmuir-Hinshelwood-Hougen-Watson and Eley-Rideal models. The activation energy was obtained 105±3.7 kJ/mol for the best fitted model. In addition the power law equation model was also evaluated for experimental data. According to the power law model the activation energy was obtained 95.5±2.5 kJ/mol. Furthermore, the effect of temperature was investigated on the reaction partial order with respect to the reactants using four simple power law equations. Characterization of the catalyst was carried out using BET and XRD techniques.

Keywords

Fe -Mn catalyst, CO hydrogenation, Kinetic investigation, characterization

1. Introduction

Fischer–Tropsch synthesis (FTS) has great potential for the production of ultraclean transportation fuels like diesel and jet fuel from synthesized gas produced from more abundant resources such as coal, natural gas and biomass. It has been found that several metals such as nickel (Ni), cobalt (Co), ruthenium (Ru) and iron (Fe) can be activated for FT reaction [1].In the High Temperature Fischer-Tropsch (HTFT) process, Sasol Company used the catalyst prepared by fused iron oxides together with the chemical and structural promoters [2]. The catalyst prepared by fused iron oxide is non-porous, so that, it obviously has lower surface area compared to other methods [3]. However, structural promoters such as the oxides of aluminum, magnesium, lanthanum, or titanium were added to increase the active surface area of the catalyst [4]. The most important catalysts prepared by this method are the promoted iron for high temperature FTS and catalysts for ammonia synthesis [3]. For iron-based catalysts, the Water-Gas-Shift (WGS) reaction can affect the FTS reaction rate by changing the hydrogen and carbon monoxide partial pressure. Addition of small amounts of manganese to the catalyst enhanced the formation of olefinic products [5]. Fe–Mn catalysts have attracted much attention due to their high olefin selectivity, lower methane selectivity, and excellent stability [5-9]. Under high reaction temperature, deactivation of catalyst may occur due to the deposition of carbon on the catalyst surface. The carbon deposits may block the catalyst pores and sites resulting in diffusion limitations and decrease activity of catalysts [10]. Temperature plays an important role in the amount of the carbon deposition on the catalyst active sites during exothermic FTS, and this reaction should be performed in way that maintains the near-isothermal conditions inside the catalyst beds [11]. Numerous studies have been reported about the FTS kinetic over the iron-based catalysts. Most kinetic expressions have been developed empirically by fitting the data to a

simple power-law relationship, It was generally found that the reaction order of hydrogen was positive, whereas that of carbon monoxide was negative [12]. Some researchers derived rate expressions of the reactant consumption based on Langmuir-Hinshelwood- Hougen-Watson (LHHW) or Eley-Rideal type mechanisms [13, 14]. One of the most popular mechanisms for the hydrocarbons formation on the iron catalysts is the surface carbide mechanism using CH_2 insertion [15-19]. Especially, iron-based catalysts form the stable carbides under FTS reaction [20, 21]. The different rate expressions proposed for the consumption of synthesis gas is mainly because of the effect of adsorbed CO, H_2, and their products (H_2O and CO_2) on the catalyst surface. Carbon monoxide and water adsorb more strongly on the catalyst surface compared to H_2 and CO_2 [22, 23]. The most evident is the usual assumption that water has a strong inhibiting influence on the reaction rate [14]. The perceived negative influence of water on the reaction rate was ascribed to the competitive adsorption between water and CO on the catalyst surface. With increasing water concentration in the surface catalyst, the fraction of CO converted to hydrocarbons decreased due to an increase in the WGS reaction. Therefore, water has essentially an indirect effect on the FTS reaction rate, and increasing the water partial pressure will reduce the amount of surface carbon, which leads to a decrease in the rate of hydrocarbon formation [24]. The following simple relationships exist between the rate of FTS reaction and WGS reaction [25].

$$r_{WGS} = r_{CO2} \quad (1)$$

$$r_{FT} = -r_{CO} - r_{CO2} \quad (2)$$

Where r_{CO2} is the rate of CO_2 formation and r_{CO} is the rate of CO consumption. Dry reported that the CO_2 inhibition is not as strong as water inhibition due to the large difference in adsorption

coefficients [23]. The negative effect of CO ascribed to an extensive coverage of the catalyst surface by adsorbed carbon monoxide and adsorption of hydrogen inhibition [24, 26].

The main objectives of the present work are to investigate the kinetic of CO hydrogenation reaction over the Fe-Mn fused catalyst and also investigate the power law equation model and obtained the kinetic parameters using these models. Furthermore, we also attempt to investigate the effect of reaction temperature on the reactant partial orders.

2. Experimental

2. 1. Catalyst preparation

The Fe-Mn catalyst used in the present work was prepared using fusion procedure. In order to prepare the fused iron catalyst the required amounts of $Fe(NO_3)_3.9H_2O$ (99% Merck), $Mn(NO_3)_2.4H_2O$ (99% Merck), La_2O_3 10 wt% (based on the total catalyst weight) and Cs_2O 1 wt% (based on the total catalyst weight) with nominal composition of 50%Fe-50%Mn-10wt% La_2O_3-1wt% Cs_2O were premixed in crucible. The obtained mixture were heated and dried at 120 °C for 14 h in an oven to give a material denoted as the catalyst precursor. The obtained precursor was fused in an electrical furnace at 1500 °C for 2 h and then cooled slowly. To prevent mass transfer limitations the obtained catalyst was crushed and screened to collect the catalysts of 30-70 mesh (210-590 μm).

2. 2. Catalysts characterization

2. 2. 1. X-Ray Diffraction (XRD)

Powder XRD measurements were performed using D5000X-ray diffraction (Siemens Germany). Scans were taken with a 2θ step size of 0.02° and a counting time of 1.0 s using a CuKα radiation source (λ=0.15406) generated at 35 KV and 20 mA. Specimens for XRD were prepared by compaction into a glass-backed aluminum sample holder. Data was collected over a 2θ range

from 5 to 70°. The line broadening of the Fe_2O_3 and MnO_2 diffraction peaks localized at 33.2° and 39° 2θ values was used to estimate the average particle sizes, according to Scherrer's equation.

2. 2. 2. BET measurements

BET surface areas, pore volumes and average pore sizes of the catalyst precursor and calcined samples (before and after the test) were measured by N_2 physisorption using a Quantachrome Nova 2000 automated system (USA). Each catalyst sample was degassed under nitrogen atmosphere at 300 °C for 3 h. In order to obtain the BET surface areas, pore volumes and average pore sizes, different samples were evacuated at -196 °C for 66 minutes.

2.3. Catalyst testing

The experiments were carried out in a fixed bed tubular stainless steel micro reactor. A schematic representation of the experimental set up is shown in Fig. 1. All gas lines to the reactor bed were made from 1/4" stainless steel tubing. Three mass flow controllers (Brooks, Model 5850E) equipped with a four-channel read out and control equipment (Brooks 0154) were used to adjust automatically the flow rate of the inlet gases (CO, H_2, and N_2 with purity of 99.999%). The mixed gases in the mixing chamber passed into the reactor tube, which was placed inside a tubular furnace (Atbin, Model ATU 150-15) capable of producing temperature up to 1500 ºC and controlled by a digital programmable controller (DPC). The reactor tube was constructed from stainless steel tubing; internal diameter of 20 mm, with the catalyst bed situated in the middle of the reactor. This single tubular micro reactor surrounded by an alumina jacket to achieve a uniform wall temperature along the length of the reactor. A preheating zone ahead of the catalyst packing was filled with inert quartz glass beads. External heating was provided by an electrical element wrapped around the alumina jacket and placed in through the firebrick part. The

required amount of the catalyst was diluted using inert silica sand with the same particle size range as the catalyst sample and placed among the inert quartz glass beads. The temperatures of all of different zones including preheating zone, catalyst bed and underneath zone of the reactor are checked by three separate thermocouples placed in different parts of the reactor. The temperature of the catalyst bed was monitored with a thermocouple located exactly in the middle of the catalyst bed. The inlet feed gas arrives from the top of the reactor and the outlet products exit from lower part of the reactor. The meshed catalyst (2.0 g) was held in middle of the reactor using quartz wool. It consist of an electronic back pressure regulator which can control the total pressure of the desired process using a remote control via the TESCOM software package integration that improve or modify its efficiency that capable for working on pressure ranging from atmospheric pressure to 100 bar. The catalyst was in situ pre-reduced at atmospheric pressure under H_2-N_2 (flow rate of each gas=50ml/min) at 350 ºC for 16 h before synthesis gas exposure. The FTS was carried out under reaction conditions of T=573–603 K, pressure of 1–15 bar, H_2/CO feed ratio of 0.7–3.4 and space velocity of 4500 h^{-1}. In each test, 2.0 g catalyst was loaded and the reactor operated about 24 h to ensure steady state operations were attained. Some experiments (reported in Table 1) were repeated for three times and comparing of the obtained results showed that steady state was achieved after 24 h. Reactant and product streams were analyzed on-line using a gas chromatograph (Thermo ONIX UNICAM PROGC+) equipped with sample loop, two Thermal Conductivity Detectors (TCD) and one Flame Ionization Detector (FID) able to perform the analysis of a wide variety of gaseous hydrocarbon mixtures, one TCD used for the analysis of hydrogen and the other one used for all the permanent gases such as N_2, O_2 and CO. The FID is used for the analysis of hydrocarbons. The system is applicable to the analysis of non-condensable gases, methane through C_8 hydrocarbons. The contents of the

sample loop were injected automatically into an alumina capillary column (30 m×0.550 mm). Helium was employed as a carrier gas for optimum sensitivity (flow rate=30 ml/min). The GC calibration was carried out using various calibration mixtures and pure compounds obtained from American Matheson Gas Company (USA).

2. 4. Heat and mass transfer limitations

Heat and mass transfer limitations are two important factors, which influence the reaction rate when heterogeneous catalysts are employed especially at high temperatures. Measuring reaction rate should not be influenced by deactivation of the catalyst or by heat and mass-transfer limitations. When the mass transfer rate is smaller than reaction rate, it results in the significant effect of mass transfer on the total observed rate or even it controls and limits the reactants transfer from the gas phase to the catalyst surface [26, 27]. In the presence of mass transfer limitations, the apparent activation energy for the reaction will be approximately one-half the true activation energy for the surface reaction [28]. Gas space velocity, catalyst particle size and catalyst amount are three important factors influencing heat and mass transfer in heterogeneous catalytic systems. With using a fixed-bed reactor, the heat and mass-transfer limitation problem could be overcome by increasing the reaction temperature and effective heat removal should be accomplished from catalytic active sites during exothermic FTS [29]. Before the kinetic experiments, mass transfer limitations in the fixed-bed reactor were investigated by changing gas space velocity and catalyst particle size. These conditions require the elimination of both pore diffusion and intra-particle (film resistance) mass transfer resistances. Preliminary experiments were performed to test the pore diffusion via decreasing the catalyst particle size. The fresh catalyst was crushed and sieved to particles with diameter of 210–590 μm (30–70 ASTM mesh) then isometric catalysts were loaded under the same operating conditions. As shown in Fig. 2, no

pore diffusion limitation was observed for particle size lower than 250 μm. By the particles size becoming smaller, the reaction rate remained constant. In the second set of experiments intra-particle mass transfer limitation (film resistance) for the reaction was investigated by variation of the space velocity (resident time) with the upstream addition of N_2 to the flow. As shown in Fig. 3, over the range of space velocity between 1500 h^{-1} to 6500 h^{-1}, with increasing the space velocity, the reaction rate remained constant and film resistance is negligible. In addition, by using a small amount of high-density catalyst (low volume) prepared by fusion method the heat and mass transfer limitations are minimized.

3. Kinetic experiments

The FTS kinetic experiments were carried out with mixture of H_2, CO and N_2 at the temperature range of 573–603 K, P=1–15 bar, H_2/CO=0.7–3.4 and GHSV=4500 h^{-1}. The required amount of the catalyst (2.0 g) was diluted using 10 g inert silica sand with the same particle size of the catalyst sample and placed among the inert quartz glass beads. For kinetic measurement tests, the reactor was operated for 24 hour until the measurements became stable. The experimental conditions and obtained data are presented in Table 1. To avoid the effect of deactivation, fresh catalysts were loaded in each experiment series. To achieve the isothermal conditions in a catalytic bed, the catalyst was diluted with inert materials (quartz and asbestos), axial temperature distribution was ensured using Mear's criterion [30, 31]. In order to avoid of channelization phenomena, the following simplified relation between catalyst bed length (Lb) and mean catalyst particle diameter (dp) was fulfilled, Lb/dp>50. We have a differential flow reactor when we choose to consider the rate to be constant at all points within the reactor. Since rates are concentration dependent this assumption is usually reasonable only for small

conversions or for shallow small reactors. For each run in a differential reactor, the plug flow performance equation becomes as follows:

$$\frac{W_{cat}}{F_{CO}^{\circ}} = \int_{X_{CO,in}}^{X_{CO,out}} \frac{dX_{CO}}{-r_{CO}} = \frac{1}{(-r_{CO})_{avg}} \int_{X_{CO,in}}^{X_{CO,out}} dX_{CO} = \frac{X_{CO,out} - X_{CO,in}}{(-r_{CO})_{avg}} \quad (3)$$

$$(-r_{CO})_{avg} = \frac{F_{CO}^{\circ}\,(X_{CO,out} - X_{CO,in})}{W_{cat}} = \frac{F_{CO,in} - F_{CO,out}}{W_{cat}} \quad (4)$$

Therefore as a brief:

$$\frac{W_{cat}}{F_{CO}^{\circ}} = \frac{X_{CO}}{-r_{CO}} \quad (5)$$

And hence:

$$-r_{CO} = \frac{X_{CO}\,F_{CO}^{\circ}}{W_{cat}} \quad (6)$$

Molar flow rate of carbon monoxide in feed is calculated from:

$$F_{CO}^{\circ} = \nu_{\circ} C_{CO} = \frac{\nu_{\circ} P_{CO}}{RT} \quad (7)$$

4. Results and discussion

4. 1. Kinetic models and rate equations

In order to obtain the rate equation, at first a reaction mechanism should be considered. For determination of kinetic models, four different mechanisms were presented according to the basis of different monomer formation and carbon chain repartition rate. The elementary reactions of these four offered mechanisms are summarized in Table 2. For derivation of each kinetic model, at first one of the elementary reaction steps was considered as rate determination step (RDS) and all other steps were assumed at equilibrium. With consideration of different RDS for the proposed models, 14 different rate expressions were obtained (presented in Table 3). Finally, all of the resulted rate expressions were fitted separately against experimental data. According to

the obtained results FT-I-1 was chosen as the best fitted model (the first step of the elementary reaction of FT-I model was considered as the RDS). The elementary reaction steps of FT-I model are presented in Table 2. The reaction rate of the RDS 1 for FT-I is:

$$-r_{CO} = k_1 P_{CO} \Theta_s^2 \quad (mol_{CO} g_{cat}^{-1} min^{-1}) \tag{8}$$

where Θ_s is referred to the fraction of free site. As can be observed in Table 2 in FT-I model the adsorbed species are C, H and O and Θ_C, $\Theta_H$and Θ_O respectively referred to the surface fraction occupied with carbon, hydrogen and oxygen which can be calculated via the site balance, the preceding reaction steps which are at quasi-equilibrium:

$$CO + 2s \rightleftharpoons C_s + O_s \tag{9}$$

$$k_1 P_{CO} . \Theta_s^2 = k_{-1} . \Theta_C . \Theta_O \tag{10}$$

$$K_1 = \frac{k_1}{k_{-1}} = \frac{\Theta_C . \Theta_O}{P_{CO} . \Theta_s^2} \tag{11}$$

$$\Theta_C . \Theta_O = \alpha P_{CO} . \Theta_s^2 \qquad , \alpha = \frac{k_1}{k_{-1}} \tag{12}$$

$$\Theta_C = \Theta_O = (\alpha P_{CO})^{0.5} \Theta_s \tag{13}$$

Where α is equilibrium constant of CO adsorption step. $\Theta_H$is obtained from below steps:

$$H_2 + 2s \rightleftharpoons 2H_s \tag{14}$$

$$k_2 P_{H_2} . \Theta_s^2 = k_{-2} . \Theta_H^2 \tag{15}$$

$$K_2 = \frac{k_2}{k_{-2}} = \frac{\Theta_H^2}{P_{H_2} . \Theta_s^2} \tag{16}$$

$$\Theta_H^2 = \left(\frac{k_2}{k_{-2}}\right) . P_{H_2} . \Theta_s^2 \qquad , \beta = \frac{k_2}{k_{-2}} \tag{17}$$

$$\Theta_H = (\beta P_{CO})^{0.5} \Theta_s \tag{18}$$

The free sites fraction (Θ_s) is calculated from the site balance:

$$\Theta_s + \sum_{i=1}^{n} \Theta_{is} = 1 \quad (19)$$

Where Θ_{is} refer to the surface fraction occupied with adsorbed species (C, H and O here). So that the site balance becomes:

$$\Theta_s + \Theta_C + \Theta_O + \Theta_H = 1 \quad (20)$$

with substituting Eqs. 13 and 18 into Eq 20, the free active sites fraction is obtained as follow:

$$\Theta_s + 2(\alpha P_{CO})^{0.5}\,\Theta_s + (\beta P_{H_2})^{0.5}\,\Theta_s = 1 \quad (21)$$

$$\Theta_s(1 + 2(\alpha P_{CO})^{0.5} + (\beta P_{H_2})^{0.5}) = 1 \quad (22)$$

$$\Theta_s = \frac{1}{(1 + 2(\alpha P_{CO})^{0.5} + (\beta P_{H_2})^{0.5})} \quad (23)$$

By substituting of eq 23 into eq 8, the rate expression is obtained:

$$-r_{CO} = \frac{KP_{CO}}{(1 + 2(\alpha P_{CO})^{0.5} + (\beta P_{H_2})^{0.5})^2} \quad (24)$$

Where $K=k_1$

The schematic representation of CO hydrogenation reaction over the Fe-Mn fused catalyst for production of different hydrocarbons according to the best fitted model with details is illustrated in Fig. 4.

4. 2. Kinetic parameters estimation

Model parameters were calculated from the experimental data and optimized with statistical indicators. The various plots provided by the Poly math software 6.0 to assess the quality of the regression models and compare the various models. The parameters that used in the Poly math software 6.0 consists of, graph, residual plot, confidence interval, R^2, R^2_{adj} Variance and R_{msd} is defined as follows:

Graph: Graph is a plot, on the bases of the calculated and measured values of R_{CO} for each proposed model. An inappropriate model shows different trends. Fig. 5 compares the R_{CO} of experimental and calculated for expression which obtained for FT-I-1 (Table 3) with assumption that the step 1 is the rate controlling step.

Residual plot: The residual plot is a plot that shows the difference between the calculated and measured values of the dependent variable as function of the measured values. The residuals between proposed model and experiment should be normally distributed with zero average line. A comparison between calculated and experimental CO conversion is presented in Fig. 6. This Figure showed that the residual relative errors (RRs) between model and experiment are mostly distributed within zero line.

Confidence interval: If the confidence interval be smaller (or at least equal) than the respective parameter values (in absolute values), then the regression model is stable and statistically valid.

R^2 and R^2_{adj}: The correlation coefficients were used to judge whether the model represents correctly the data. These parameters defined as Eqs 25-27.

$$\overline{y} = \frac{1}{n}\left(\sum_{i=1}^{n} yi_{exp}\right) \quad (25)$$

$$R^2 = 1 - \frac{\sum_{i=1}^{n}(yi_{\exp} - yi_{calc})^2}{\sum_{i=1}^{n}(yi_{\exp} - \overline{y})} \quad (26)$$

$$R^2{}_{adj} = 1 - \frac{(1 - R^2)(n-1)}{n - p} \quad (27)$$

In above formulas the notation n, y_i ,exp and calc are denotes to the number of experimental, specific observation, observed data and calculated data respectively.

Variance and R_{msd}: Variance and R_{msd} are defined as Eqs (28) and (29).

$$S^2 = \frac{\sum_{i=1}^{n}(y_i - \overline{y})^2}{(n-1)} \quad (28)$$

$$R_{msd} = \frac{1}{n}\left[\sum_{i=}^{n}(yi_{\exp} - yi_{calc})^2\right]^2 \quad (29)$$

Some statically indicators that used to assess the quality of the proposed model (expression FT-I, RDS 1) in Table 3 are summarized in Table 4.

For estimation of the best kinetic model we assumed that:

1- The mass transport limitations and pressure drop are connivance.

2- The suitable values for all parameters must be positive and all offered models with negative values parameters will refused.

Estimation of parameter and model distinction have accomplished by nonlinear regression model and using of poly math software 6.0. Fig. 6 displayed the residuals between offered model and experimental data distributed randomly around zero line. This Figure confirmed that the offered model is in good agreement with the experimental data.

According to the obtained results the best expression that described the experimental results for FT reaction over Fe-Mn fused catalyst is as follow (Eq. 24):

$$-R_{CO} = \frac{KP_{CO}}{(1+2(\alpha P_{CO})^{0.5} + (\beta P_{H_2})^{0.5})^2}$$

Kinetic and adsorption parameters which depend on temperature described and calculated according to the Arrhenius and Van't Hoff equations respectively (Eqs. 30 & 31):

$$k_i(T) = k_{i,0} exp\,(-E_i)/RT \quad (30)$$

$$\alpha(T) = \alpha_0 exp\,(-\Delta H_{ads})/RT \quad (31)$$

In these equations E and ΔH refers to the activation energy and heat of adsorption respectively; by substituting Eqs. (30) and (31) in the best fitted model (FT-I-1) we have:

$$-\mathrm{R_{CO}} = \frac{(\mathrm{K_{i,0}}\exp(-\mathrm{E_i})/\mathrm{RT})\,\mathrm{P_{CO}}}{(1+2(\propto_0 \exp(-\Delta \mathrm{H_{co}})/\mathrm{RT})\mathrm{P_{CO}})^{0.5} + (\beta_0 \exp(-\Delta H_{H2})/RT)P_{H_2})^{0.5})^2} \quad (32)$$

The relation between the temperature and reaction rate constant according to the kinetic parameters obtained from FT-I-1 model is shown in Fig. 7. According to the Arrhenius-type equation (Eq. 30), a plot of ln(k) versus 1/T should give a straight line with negative slope of $-E_i/R$. The relation between the temperature and adsorption enthalpy (Van't Hoff plot) for the FT-I-1 model, is shown in Fig. 8.

The mean absolute relative residual (MARR%) between experimental and calculated consumption rate of CO is defined as:

$$\text{MARR}\ (\%) = \sum_{i=1}^{N_{exp}} \left| \frac{r_{exp} - r_{cal}}{r_{exp}} \right| \times \frac{1}{N_{exp}} \times 100 \qquad (33)$$

Where, N_{exp} is the number of experimental points. Eq. 24 shows the best fit to the experimental data. The comparison of the calculated and experimental consumption rate of CO for the FT-I-1 model is shown in Fig. 9 and the MARR% of this model was obtained 5.50%. This value is reasonable and shows that the predicted values are 5.50% different from the observed values. The MARR% values of the other obtained kinetic models are presented in Table 3; as can be seen in this Table the FT-I-1 model has the minimal MARR% value. The obtained activation energy for FT-I-1 was found to be 105 ±3.7 kJ/mol.

4. 2. Kinetic investigation using power law model

The effect of reactants on the reaction rate was investigated by many researchers [12, 22, 24-26, 32-34]. In the present work, we attempted to investigate the relationship between reactants partial pressure and temperature changes. By using the power law equation (Eq. 34), the order of reaction was obtained at four temperatures for FTS. To investigate the effect of water on the reaction rate, water pressure was entered in the power law equation:

$$r_{FT} = k_{FT}.P_{CO}^{a}.P_{H_2}^{b}.P_{H_2O}^{c} \qquad (34)$$

The obtained results are summarized in Table 5. The obtained results showed that along with increasing temperature from 573 to 603 K the partial orders of CO and H_2O were increased and the partial order of hydrogen was decreased. The effect of temperature on the reaction order is plotted in Fig. 10. Previous research works showed that the reaction order of H_2 [b] was positive but the reaction orders of CO [a] and H_2O [c] were negative [23, 24, 35]. It could be argued that the higher CO partial pressure leads to higher coverage of catalyst surface by adsorbed CO. As it shown in Fig. 10 by increasing temperature the reaction order was changed for all reactants. Along with increasing temperature, adsorbed CO molecules are consumed more rapidly and so the numbers of free active sites for adsorption of H_2 molecules are increased. Increasing in the free active sites numbers leads to easier adsorption of hydrogen molecules on the catalyst surface; so that the positive effect of higher H_2 partial pressure on the reaction rate was decreased. The calculated activation energy for CO hydrogenation reaction according to the power law model was found to be 95.54±2.5 kJ/mol; the high activation energy for hydrocarbon formation suggests that the diffusion interference is not significant in the experiments [36,37]. As with intra-particle diffusion limitations, the presence of external mass-transfer limitations could be detected via measuring the apparent activation energy. An external mass-transfer control regime could lead to the apparent activation energy of just a few kJ/mol [38].

According to the power law equation (Eq. 34) four rate constant (k) were obtained for 4 different temperatures (Table. 6). In order to show the relationship between the reverse of temperature and the logarithm of the rate constant obtained from this model; Arrhenius equation (Eq. 30) was used. The obtained plot displayed in Fig. 11 showed this relationship and show the straight line with the negative slope ($-E_a/R$). The value of -E/R was found to be -11492 which yields activation energy of 95.54 kJ /mol.

The kinetic parameters and activation energy of the power law model (Eq. 34) were calculated and the obtained results are presented in Table 6. The comparison of the calculated and experimental consumption rate of CO for the Eq. 34 is shown in Fig. 12 and the MARR% of this model was obtained 8.86%. This value is reasonable and shows that the predicted values are 8.86% different from the observed values. Fig. 13 shows comparison between experimental and calculated intrinsic reaction rates using power law equation.

4. 1. Catalysts characterization

Characterization of the fresh catalyst (sample before the test) and used sample (catalyst after the test) was carried out using powder X-ray diffraction and the obtained patterns are illustrated in Fig. 14. The actual phases identified in the fresh catalyst, were Fe_2O_3 (Hexagonal), MnO_2 (Tetragonal), Fe_3O_4 (cubic) and Mn_2O_3 (Orthorhombic). In order to identify the changes in the catalyst during the reaction and to detect the phases formed this catalyst was characterized by XRD after the test and its phases were found to be MnO (cubic), FeO (cubic), Fe (cubic) and Fe_2C (monoclinic). As can be seen, in the tested catalyst there are oxidic and iron carbide phases, which are both active for FTS. Zhang and Schrader [39] concluded that two active sites operate simultaneously on the surface of iron catalysts: Fe0/Fe-carbides and magnetite (Fe_3O_4). The carbide phase is active towards dissociation of CO and formation of hydrocarbons, while the oxide phase adsorbs CO associatively and produces predominantly oxygenated products. The crystallite size of fresh catalyst was calculated by Debye-Scherrer equation from XRD data. Average crystallite sizes for Fe_2O_3 and MnO_2 were calculated 91and 83 nm respectively.

Characterization of fresh catalyst was also carried out using BET measurements; the obtained results showed that the surface area of this sample was 14 m^2/g. The area of catalyst can be improved during reduction process partially [3, 5]. Addition of Mn appeared to increase the BET

surface area of the Fe catalysts [4]. Dry has suggested that alkali promoter can decrease the surface area of the Fe catalyst by increasing the Fe crystallite size [40].

5. Conclusion

Kinetic of the CO hydrogenation reaction was investigated over the fused Fe-Mn catalyst in a fixed bed micro reactor over a range of operating conditions. Four different mechanisms according to the carbide mechanism using Langmuir-Hinshelwood-Hougen-Watson and Eley-Rideal are derived for CO hydrogenation. The unknown kinetic parameters were estimated from experimental data using non-linear regression (Levenberg–Marquardt) method. The reaction rate of CO hydrogenation is determined by the formation of the methylene monomer. In the best fitted model (FT-I-1) both reactant (CO and H_2) were dissociated and adsorbed on the catalyst surface. Furthermore, the power law model was also proposed and evaluated. The present work results also showed that along with increasing the reaction temperature the reaction partial orders of all reactants were changed.

Nomenclature

r_{FT}: rate of reaction

r_{WGS}: rate of water gas shift reaction

r_{CO}: rate of CO consumption

r_{CO2}: rate of CO_2 production

$F°_{CO}$: Inlet Molar Flow of CO

ν_o: Volumetric Flow Rate of Input Gas

C_{CO}: Concentration of CO

P_{CO}: Partial Pressure of CO

P_{H2}: Partial Pressure of H_2

P_{H2O}: Partial Pressure of H_2O

T: Gas Temperature

R: Universal Gas Constant

k: rate constant of reaction

E_a: activation energy

α: adsorption coefficient of CO

β: adsorption coefficient of H_2

ΔH_{H2}: adsorption enthalpy of H_2

ΔH_{CO}: adsorption enthalpy of CO

X_{CO}: the conversion of CO

W: the catalyst weight

Reference

[1] N. Moazami, M. L. Wyszynski, H. Mahmoudi, A. Tsolakis, Z. Zou, P. Panahifar, K. Rahbar, Fuel, 2015, **154**,140–151.

[2] A. P. Steynberg, M. E. Dry, Fischer-Tropsch technology, Elsevier Science & Technology Books, 2004, p 533.

[3] M. S. Spencer, in: M. V. Twigg (Eds.) Catalyst Handbook ,Wolfe Publishing Ltd, London, 1989, p. 35.

[4] M. E. Dry, J. A. K. Plessis, G. M. Leuteritz, J. Catal. 1966, **6**, 194-199.

[5] G. C. Maiti, R. Malessa, U. Lochner, H. Papp, M. Baerns, Appl. Catal. A. General. 1985, **16**, 215-225.

[6] B. Liu, J. Zhang, W. Cao, X. Yang, Fuel Process .Technol. 2009, **90**, 1480-1485.

[7] C. H. Zhang, Y. Yang, B. T. Teng, T. Z. Li, H. Y. Zheng, H. W. Xiang, Y. W. Li, J. Catal. 2006, **237**, 405-415.

[8] F. Fazlollahi, M. Sarkari, H. Gharebaghi, H. Atashi, M. M. Zarei, A. A. Mirzaei, W. C. Hecker, Chin. J. Chem. Eng, 2013, **21**, 507-519.

[9] X. Zhang, Y. Liu, G. Liu, K. Tao, Q. Jin, F. Meng, D. Wang, N. Tsubaki, Fuel. 2012, **92**,122-129.

[10] D. J. Moodley, J. v. d. Loosdrecht, A. M. Saib, H. J. W. Niemantsverdriet, in: B. H. Davis, M. L. Occelli (Eds.) Advances in Fischer-Tropsch Synthesis, Catalysts, and Catalysis, CRC Press, Boca Raton, 2010, p. 53.

[11] C. H. Bartholomew, Mechanisms of catalyst deactivation, Appl. Catal. A. General 2001, **212**,17-60.

[12] T. K. Das, X. Zhan, J. Li, G. Jacobs, M. E. Dry, B. H. Davis, in: B. H. Davis, M. L. Occelli (Eds.) Fischer-Tropsch Synthesis, Catalysts and Catalysis, Elsevier B.V., 2007, p. 298.

[13] G. P. V. d. Laan, A. A. C. M. Beenackers, Catal .Rev.: Sci. Eng. 1999, **41**, 255-318.

[14] F. G. Botes, Catal. Rev.: Sci. Eng. 2008, **50**, 471-491.

[15] A. Nakhaei Pour, M. R. Housaindokht, S. F. Tayyari, J. Zarkesh, M. R. Alaei, J. Nat. Gas Sci. Eng, 2010, **2**, 61-68

[16] M. Sarkari, F. Fazlollahi, H. Ajamein, H. Atashi, W. C. Hecker, L. L. Baxter, Fuel. Proc. Tech. 2014, **127**, 163–170

[17] G. P. V. d. Laan., A. A. C. M. Beenackers, Appl. Catal. A. General, 2000, **193**, 39-53.

[18] Y. N. Wang, W. P. Ma, Y. J. Lu, J. Yang, Y. Y. Xu, H. W. Xiang, Y. W. Li, Y. L. Zhao, B. J. Zhang, Fuel, 2003, **82**, 195-213.

[19] B. T. Teng, J. Chang, C. H. Zhang, D. B. Cao, J. Yang, Y. Liu, X. H. Guo, H. W. Xiang, Y. W. Li, Appl. Catal. A. General, 2006, **301**, 39-50.

[20] W. Erley, P. H. Mcbreen, H. Ibach, J. Catal. 1983, **84**, 229-234.

[21] B. H. Davis, Catal. Today, 2009, **141**, 25-33.

[22] F. G. Botes, B. B. Breman, Ind. Eng. Chem. Res, 2006**, 45**, 7415-7426.

[23] M. E. Dry, T. Shingles, L. J. Boshoff, G. J. Oosthuizen, J. Catal. 1969, **15**, 190-199.

[24] E.v. Steen, H. Schulz, Appl. Catal. A. 1999, **186**, 309-320.

[25] V. R. R. Pendyala, G. Jacobs, J. C. Mohandas, M. Luo, W. Ma, M. K. Gnanamani, B. H. Davis, Appl. Catal. A. General, 2010, **389**,131-139.

[26] F. G. Botes, Ind. Eng. Chem. Res. 2009, **48**,185-1865.

[27] X. Zhan, B. H. Davis, Appl. Catal. A.General, 2002, **236**,149-161.

[28] P. Schneider, P. Mitschka, Chem. Eng. Sci. 1969, **24**, 1725-1731.

[29] H. J. Kim, J. H. Ryu, H. Joo, J. Yoon, H. Jung, J. I. Yang, Res. Chem. Intermed, 2008, **34**, 811-816.

[30] D. E. Mears, ACS Monographs. 1974, **133**, 218–228.

[31] M. Mollavali, F. Yaripour, H. Atashi, S. Sahebdelfar, Ind. Eng. Chem. Res. 2008, **47**, 3265–3273.

[32] D. Tristantini, S. Lögdberg, B. Gevert, O. Borg, A. Holmen, Fuel Proc. Tech, 2007, **88**, 643-649.

[33] S. Storsaeter, O. Borg, E. A. Blekkan, A. Holmen, J. Catal, 2005, **231**, 405-419.

[34] R. Zennaro, M. Tagliabue, C. H. Bartholomew, Catal. Today, 2000, **58**, 309–319

[35] M. Zhuo, A. Borgna, M. Saeys, J. Catal. 2013, **297**, 217-226.

[36] A. Sari, Y. Zamani, S. A. Taheri, Fuel Proc. Tech. 2009, **90**, 1305– 1313.

[37] J. Chang, L. Bai, B. T. Teng, R. Zhang, J. Yang, Y. Y. Xu, H. W. Xiang, Y. W. Li, Chem. Eng. Sci, 2007, **62**, 4983–4991.

[38] A. Y. Khodakov, W. Chu, P. Fongarland, Chem. Rev, 2007, **107**, 1692–1744.

[39] H. B. Zhang, G. L. Schrader, J. Catal, 1985, **95**, 325-332.

[40] M. E. Dry, G. J. Oosthuizen, J. Catal, 1968, **11**, 18-24.

Caption to Figures

Figure 1. Schematic representation of the reactor in a flow diagram used. 1- Gas cylinders, 2- Pressure regulators, 3- Needle valves, 4- Ball valves, 5- Mass Flow Controllers (MFC), 6- Digital pressure controllers, 7- Pressure gauges, 8- Non return valves, 9- Mixing chamber, 10- Valves, 11- Tubular furnace, 12- Tubular reactor and catalyst bed, 13- Temperature indicators (Digital Program Controller), 14- Resistance Temperature Detector (RTD), 15- Condenser, 16- Trap Air, 17- BPR: Back Pressure Regulator, 18- Flow meter, 19- Silica gel column 20- Gas Chromatograph (GC), 21-Hydrogen generator**.**

Figure 2. Variation of reaction rate as a function of particle size; Conditions: T=603K, P=1bar, GHSV=3600h^{-1}.

Figure 3. Variation of reaction rate as a function of GHSV value; Conditions: T=603K, P=1bar.

Figure 4. schematic description of FT mechanism according to the FT-I-1 model.

Figure 5. Comparison between experimental and calculated reaction rate using Eq. (8). Reaction conditions: T=573-603K, P=1–15 bar, H_2/CO=1/1–3/1 and GHSV=4500 h^{-1}.

Figure 6. The relative residuals for CO consumption rate (• Rexp - Rcal).

Figure 7. Arrhenius plot of rate constant (k) according to the FT-I-1 model results

Figure 8. Van't Hoff plots of coefficient adsorption of (A) CO molecule & (B) H_2 molecule according to the obtained results from the FT-I-1 model.

Figure 9. The calculated CO consumption rate versus the experimental CO consumption rate for FT-I-1 model.

Figure 10. Effect of reaction temperature on the reaction partial orders.

Figure 11. Arrhenius plot according to the power law equation results.

Figure 12. The calculated CO consumption rate versus the experimental CO consumption rate using power law model.

Figure 13. Comparison between experimental and calculated reaction rate for power law equation (Eq. 34).

Figure 14. XRD patterns of calcined catalysts (before and after the test).

Caption to Tables

Table 1. Experimental conditions for kinetic evaluations at P_{tot}=1–15 bar, T=573–603 K, H_2/CO=1-3 and GHSV=4500 h^{-1} in a fixed bed reactor (FBR).

Table 2. Reaction schemes of CO hydrogenation

Table 3. Reaction rate expressions for CO hydrogenation.

Table 4. Obtained values of kinetic parameters for the fitted model (FT-I-1) and statistical criteria.

Table 5. The obtained results for the reaction order using power law equation, at different temperatures (573-603K).

Table 6. Values of kinetic parameters for the power law model (Eq. 34).

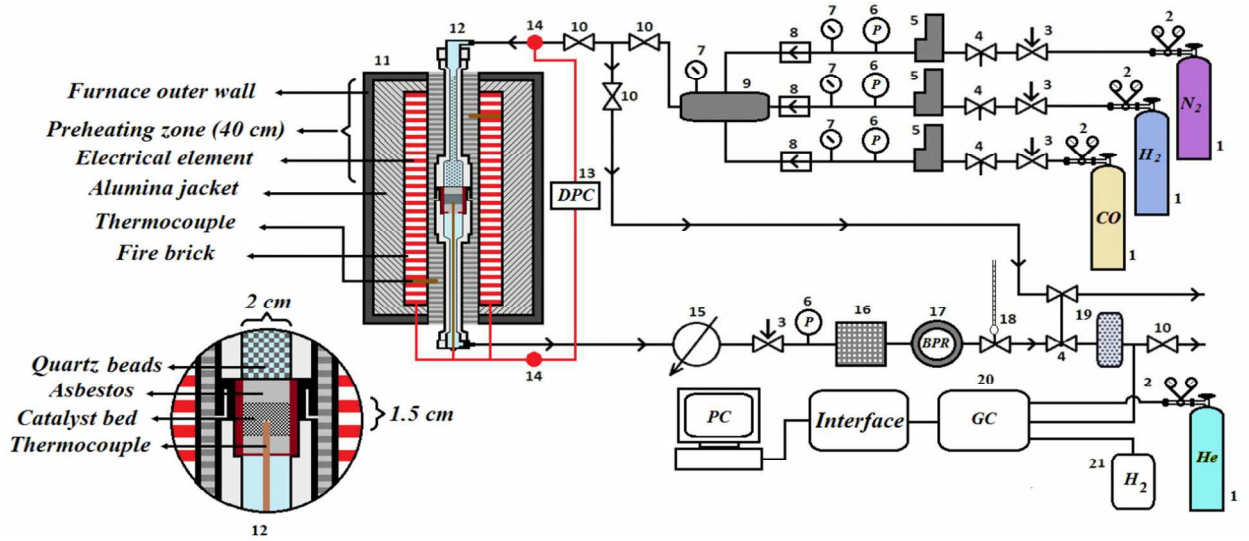

Figure 1

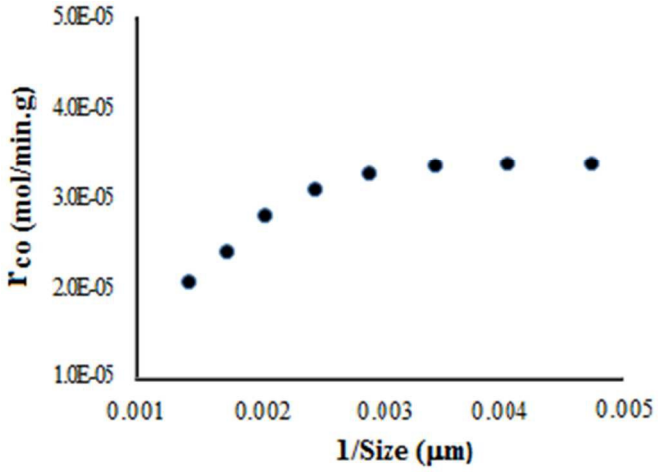

Figure 2

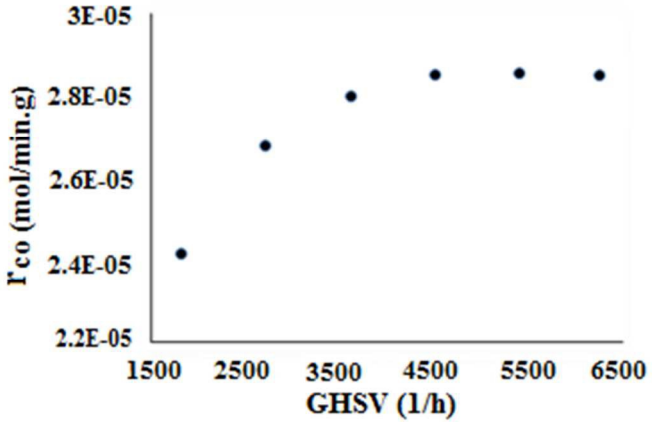

Figure 3

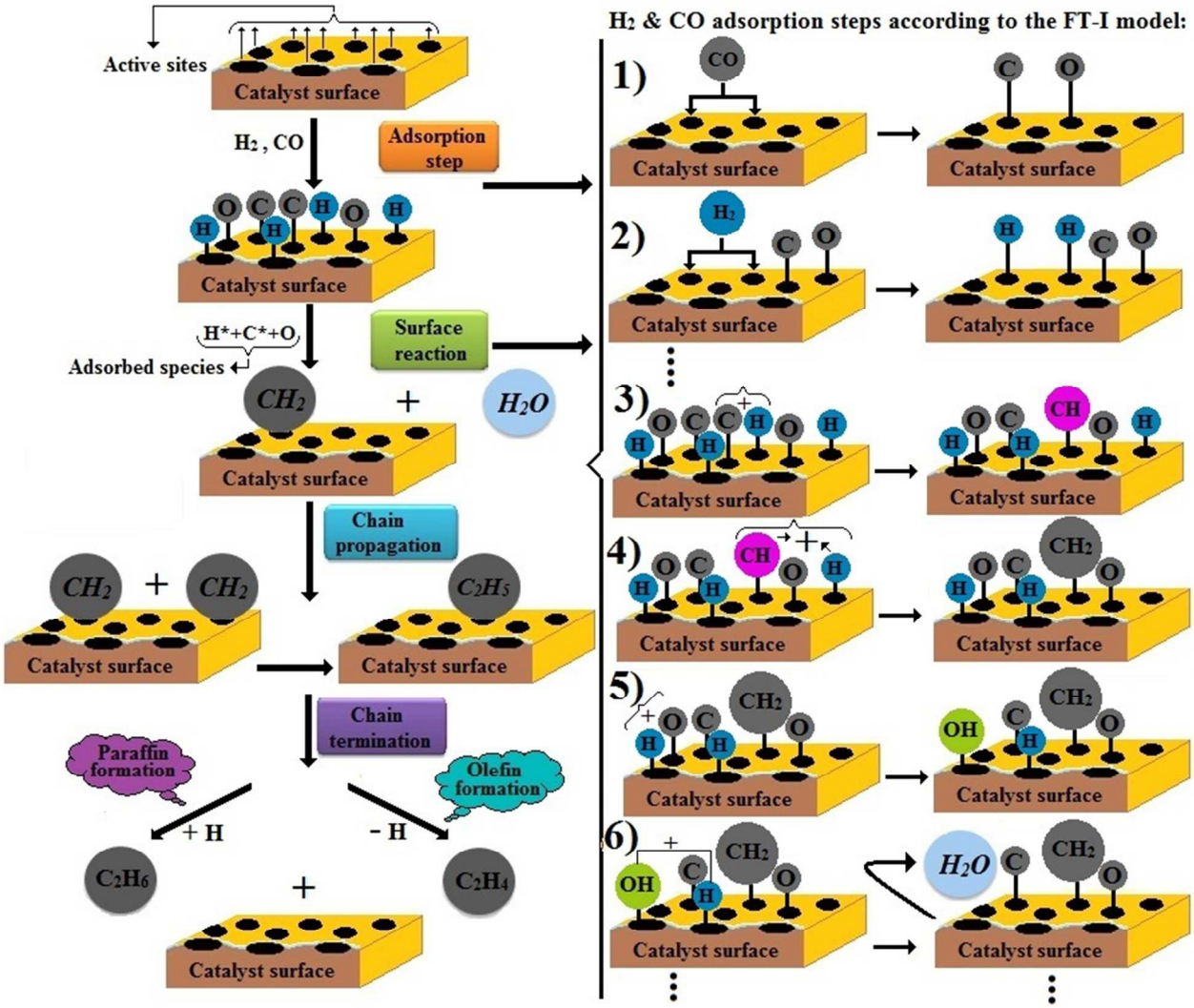

Figure 4

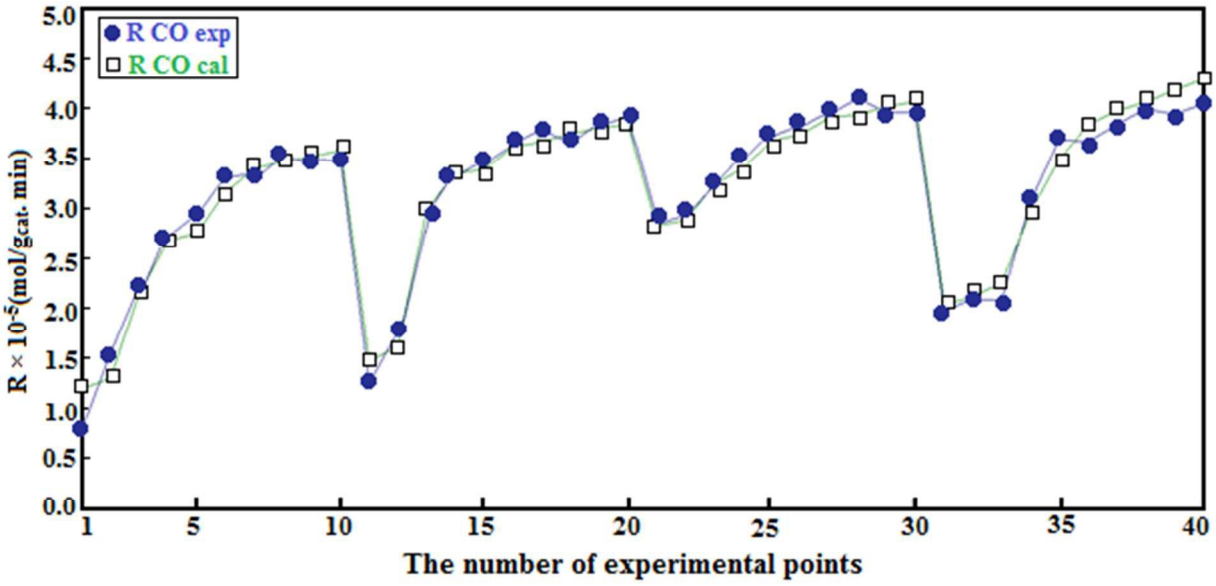

Figure 5

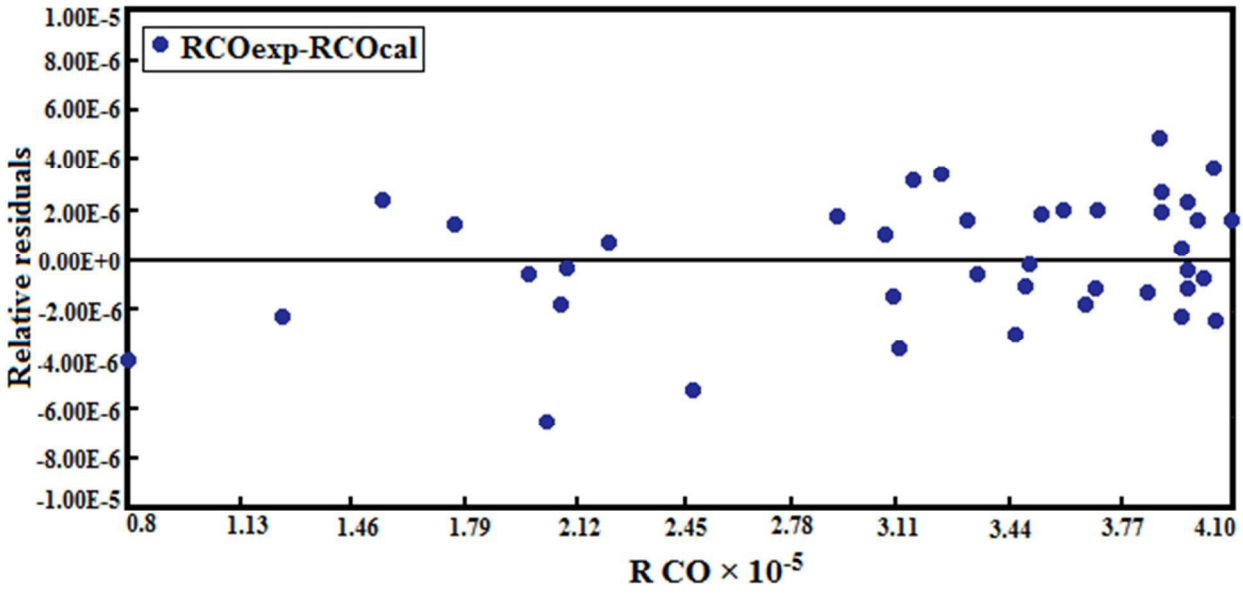

Figure 6

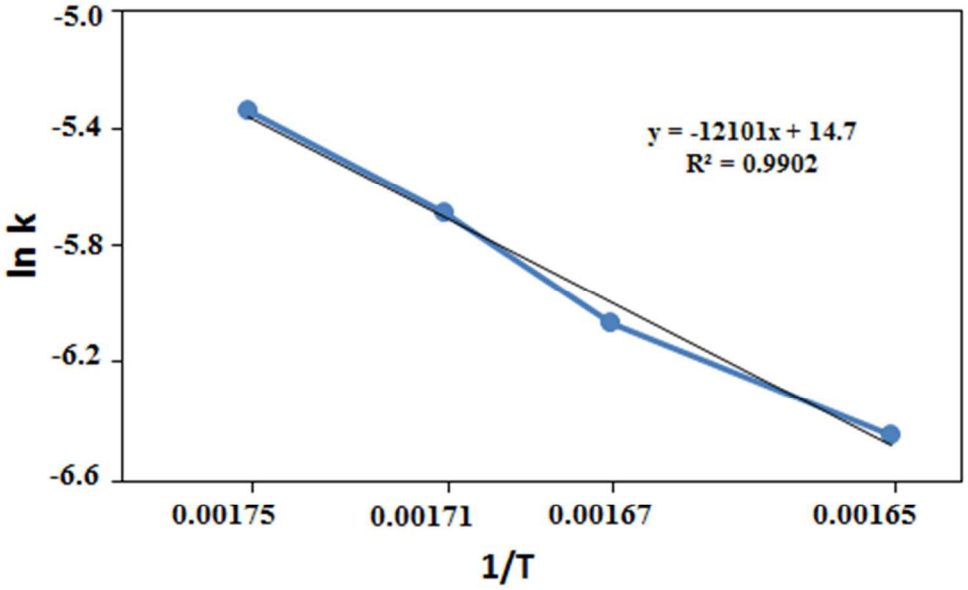

Figure 7

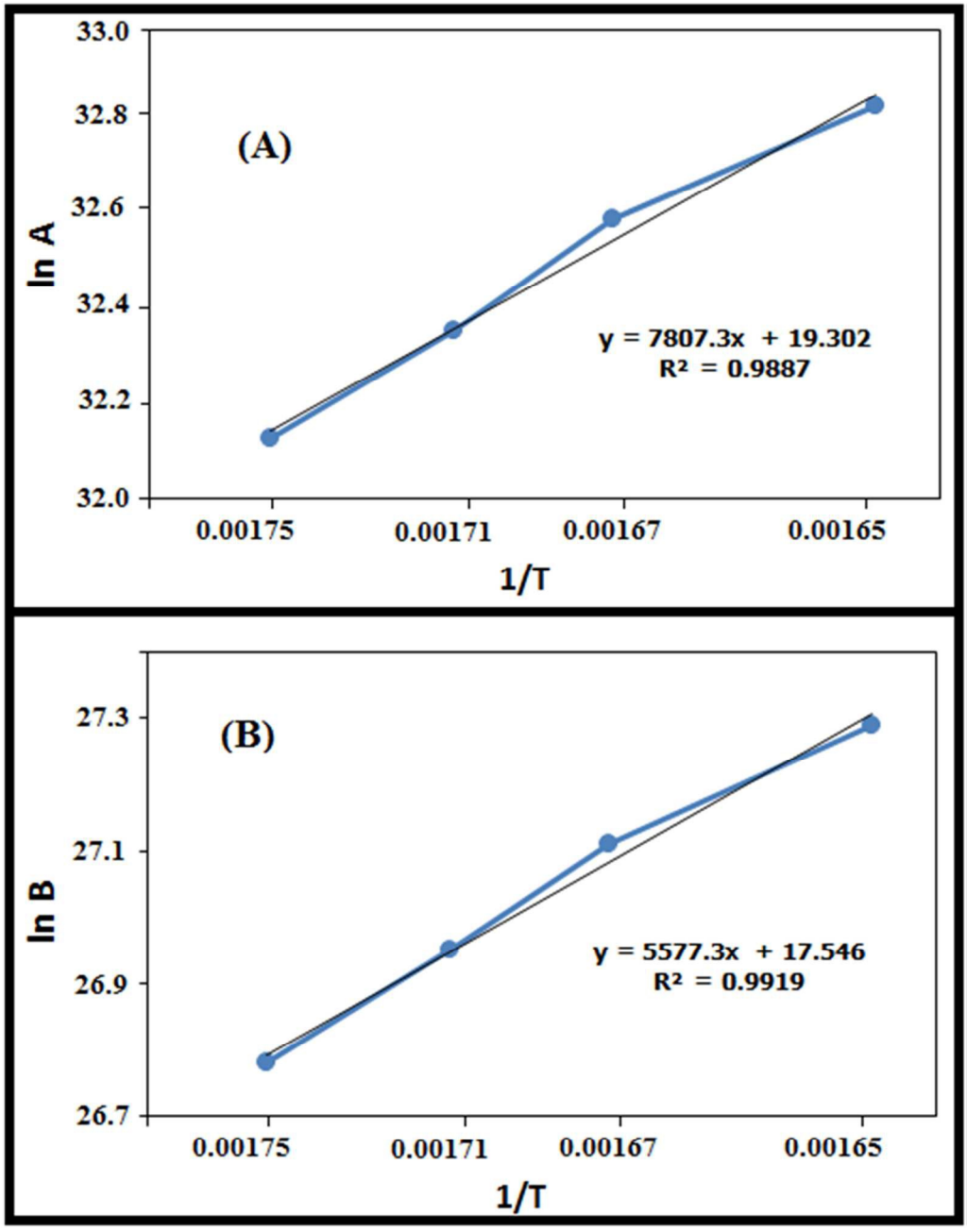

Figure 8

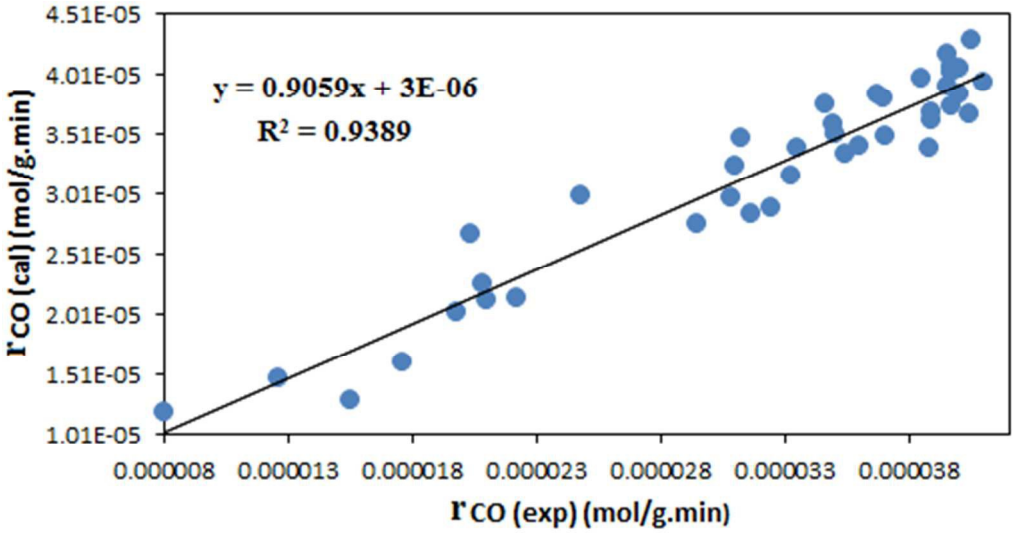

Figure 9

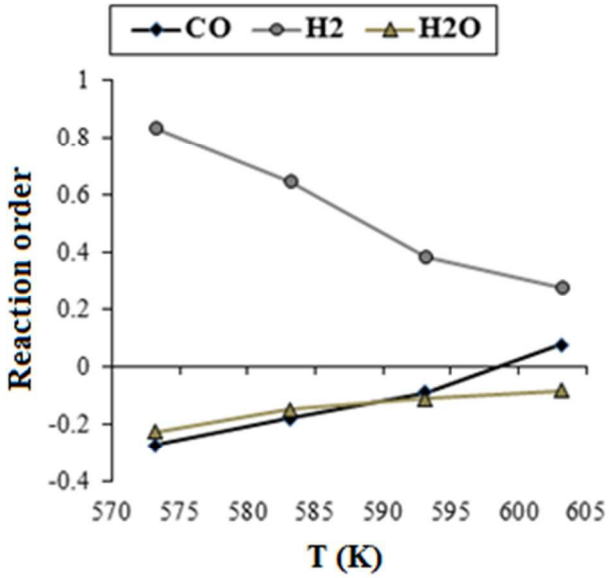

Figure 10

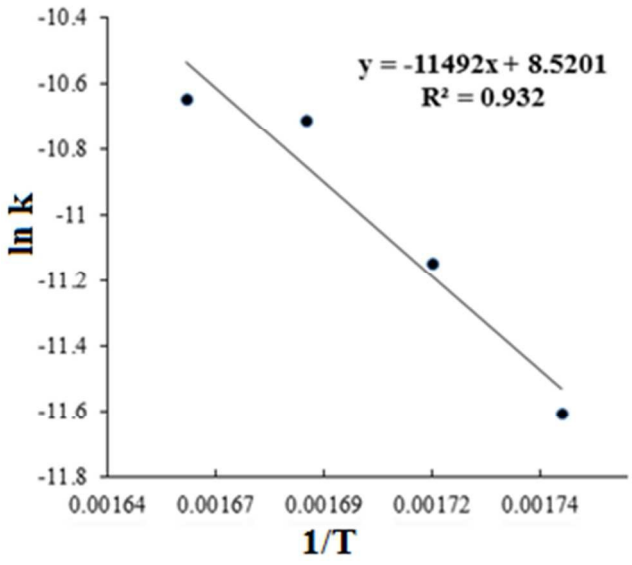

Figure 11

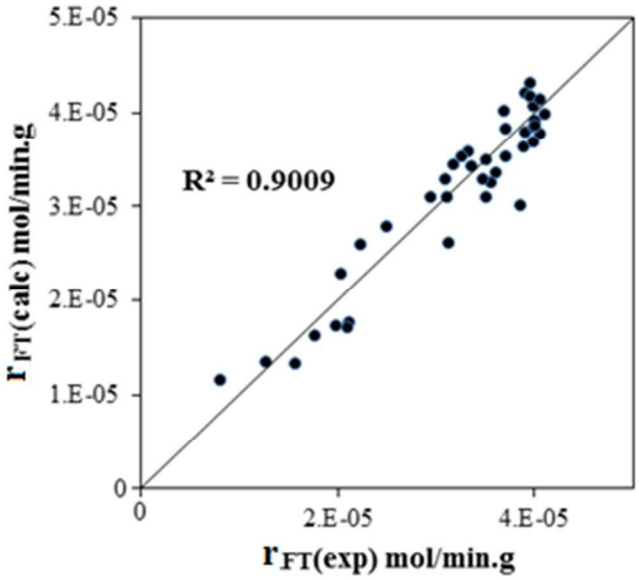

Figure 12

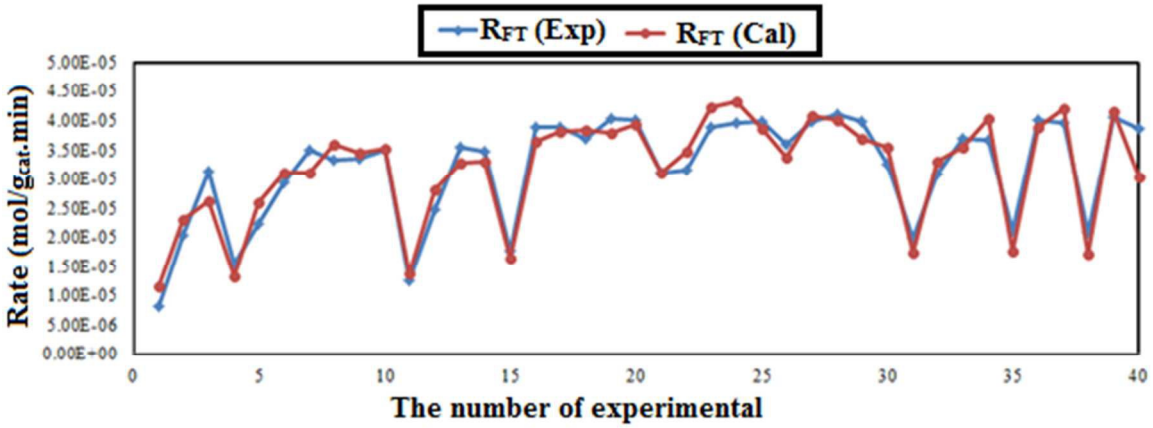

Figure 13

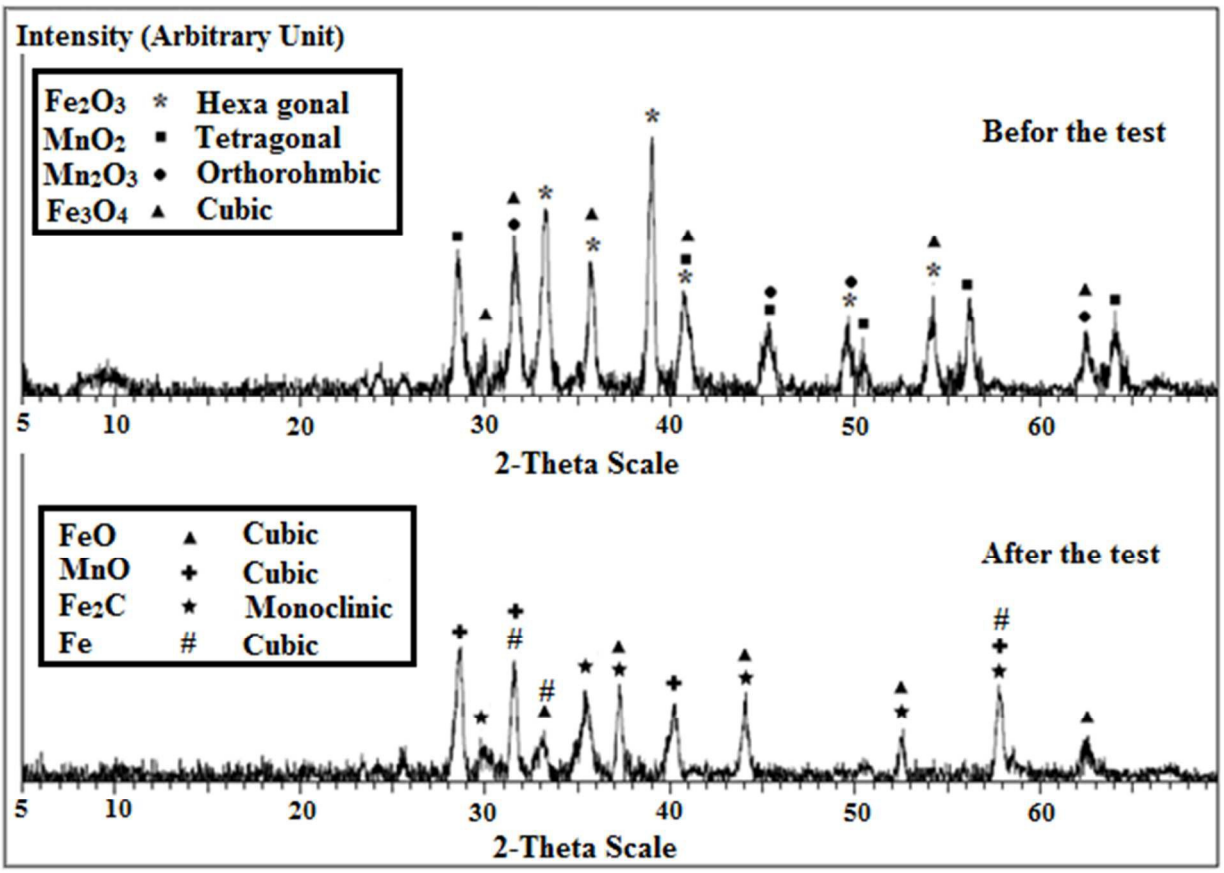

Figure 14

NO	T (K)	P_{total} (bar)	H_2/CO	P_{CO} (bar)	P_{H2} (bar)	P_{H2O} (bar)	R (mol/min g_{cat})
1*	573.15	1	0.97	0.38	0.37	0.03	8.00E-06
2	573.15	1	1.95	0.22	0.43	0.04	1.55E-05
3	573.15	3	1.97	0.64	1.26	0.11	2.22E-05
4*	573.15	6	1.02	2.27	2.32	0.17	2.03E-05
5	573.15	6	2.02	1.25	2.53	0.25	2.94E-05
6	573.15	9	3.15	1.27	4.00	0.46	3.32E-05
7*	573.15	12	3.19	1.66	5.30	0.70	3.35E-05
8	573.15	15	1.04	5.54	5.76	0.36	3.12E-05
9	573.15	15	2.03	3.00	6.10	0.80	3.50E-05
10	573.15	15	3.33	2.00	6.65	0.90	3.49E-05
11*	583.15	1	0.95	0.38	0.36	0.03	1.26E-05
12	583.15	1	1.95	0.22	0.43	0.03	1.76E-05
13	583.15	6	0.99	2.25	2.22	0.19	2.48E-05
14	583.15	9	1.03	3.25	3.36	0.21	3.54E-05
15*	583.15	9	1.97	1.78	3.51	0.45	3.88E-05
16	583.15	12	1.97	2.39	4.70	0.60	3.89E-05
17	583.15	12	3.25	1.54	5.00	0.75	4.04E-05
18	583.15	15	1.03	5.39	5.55	0.42	3.46E-05
19*	583.15	15	2.03	2.93	5.95	0.80	3.69E-05
20	583.15	15	3.34	1.86	6.22	0.93	4.00E-05
21	593.15	3	2.00	0.62	1.24	0.14	3.16E-05
22	593.15	3	3.07	0.43	1.32	0.15	3.24E-05
23*	593.15	6	0.91	2.20	2.00	0.23	3.10E-05
24	593.15	6	3.05	0.80	2.44	0.43	3.60E-05
25	593.15	9	1.99	1.76	3.50	0.50	3.89E-05
26	593.15	9	3.28	1.15	3.77	0.60	3.97E-05
27*	593.15	12	2.05	2.29	4.70	0.70	3.95E-05
28	593.15	12	3.36	1.49	5.00	0.86	4.10E-05
29	593.15	15	1.96	2.84	5.56	1.00	3.97E-05
30	593.15	15	3.37	1.78	6.00	1.15	3.97E-05
31*	603.15	1	0.89	0.37	0.33	0.03	1.98E-05
32	603.15	1	1.85	0.20	0.37	0.03	2.10E-05
33	603.15	1	2.87	0.15	0.43	0.04	2.08E-05
34*	603.15	3	0.91	1.10	1.00	0.10	3.08E-05
35	603.15	6	0.88	2.15	1.90	0.27	3.70E-05
36	603.15	9	0.94	3.20	3.00	0.40	3.67E-05
37*	603.15	12	0.74	5.00	3.70	0.80	3.85E-05
38	603.15	12	1.88	2.23	4.20	0.90	4.00E-05
39	603.15	15	1.82	2.74	5.00	1.00	3.95E-05
40*	603.15	15	3.33	1.80	6.00	1.20	4.05E-05

*: experiments repeated for three times

Table 1

Model	Number	Elementary Reaction
FT-I	1	$CO + 2s \leftrightarrow Cs + Os$
	2	$H_2 + 2s \leftrightarrow 2Hs$
	3	$Cs + Hs \leftrightarrow HCs + s$
	4	$HCs + Hs \leftrightarrow H_2Cs + s$
	5	$Os + Hs \rightarrow HOs + s$
	6	$HOs + Hs \rightarrow H_2O + 2s$
FT-II	1	$CO + s \leftrightarrow COs$
	2	$H_2 + 2s \leftrightarrow 2Hs$
	3	$COs + Hs \leftrightarrow HCOs + s$
	4	$HCOs + H_s \leftrightarrow Cs + H_2O + s$
	5	$Cs + H_s \leftrightarrow CHs + s$
	6	$CHs + H_s \leftrightarrow CH_2s + s$
	7	$O_s + H_s \leftrightarrow HO_s + s$
	8	$HO_s + H_s \rightarrow H_2O + 2s$
FT-III	1	$CO + s \leftrightarrow COs$
	2	$COs + H_2 \leftrightarrow H_2COs$
	3	$H_2COs + H_2 \leftrightarrow CH_2s + H_2O$
FT-IV	1	$CO + s \leftrightarrow Cos$
	2	$H_2 + s \leftrightarrow H_2s$
	3	$Cos + H_2s \leftrightarrow H_2Cos + s$
	4	$H_2Cos + H_2s \leftrightarrow H_2O + s$

Table 2

Number of proposed model	Rate equation	Parameters	MARR (%)
FT-I-1	$-R_{CO} = \frac{K \,.\, P_{CO}}{[1 + 2(\alpha\, P_{CO})^{0.5} + \ (\beta P_{H_2})^{0.5}]^2}$	$K = \mathrm{k}_1$ $\alpha = \frac{k_1}{k_{-1}}$ $\beta = \frac{k_2}{k_{-2}}$	5.50
FT-I-2	$-R_{CO} = \frac{K \,.\, P_{H_2}}{[1 + 2(\alpha\, P_{CO})^{0.5} + \ (\beta P_{H_2})^{0.5}]^2}$	$K = \mathrm{k}_2$ $\alpha = \frac{k_1}{k_{-1}}$ $\beta = \frac{k_2}{k_{-2}}$	10.62
FT-I-3	$-R_{CO} = \frac{K \,.\, P_{CO}^{0.5} \,.\, P_{H_2}^{0.5}}{[1 + 2(\alpha\, P_{CO})^{0.5} + \ (\beta P_{H_2})^{0.5}]^2}$	$\mathrm{K} = \mathrm{k}_3.\mathrm{K}_1^{0.5}.\mathrm{K}_2^{0.5}$ $\alpha = \frac{k_1}{k_{-1}}$ $\beta = \frac{k_2}{k_{-2}}$	8.15
FT-I-4	$-R_{CO} = \frac{K \,.\, P_{CO}^{0.5} \,.\, P_{H_2}}{[1 + 2(\alpha\, P_{CO})^{0.5} + \ (\beta P_{H_2})^{0.5}]^2}$	$\mathrm{K} = \mathrm{k}_4.\mathrm{K}_3\mathrm{K}_2\mathrm{K}_1^{0.5}$ $\alpha = \frac{k_1}{k_{-1}}$ $\beta = \frac{k_2}{k_{-2}}$	15.54
FT-II-1	$-R_{CO} = \frac{K \,.\, P_{CO}}{1 + \alpha\, P_{CO} + \ (\beta P_{H_2})^{0.5}}$	$K = \mathrm{k}_1$ $\alpha = \frac{k_1}{k_{-1}}$ $\beta = \frac{k_2}{k_{-2}}$	12.14
FT-II-2	$-R_{CO} = \frac{K \,.\, P_{H_2}}{1 + \alpha\, P_{CO} + \ (\beta P_{H_2})^{0.5}}$	$K = \mathrm{k}_2$ $\alpha = \frac{k_1}{k_{-1}}$ $\beta = \frac{k_2}{k_{-2}}$	17.67
FT-II-3	$-R_{CO} = \frac{K \,.\, P_{CO} \,.\, P_{H_2}^{0.5}}{[1 + \alpha\, P_{CO} + \ (\beta P_{H_2})^{0.5}]^2}$	$K = \mathrm{k}_3.K_1.K_2$ $\alpha = \frac{k_1}{k_{-1}}$ $\beta = \frac{k_2}{k_{-2}}$	22.43
FT-II-4	$-R_{CO} = \frac{K \,.\, P_{H_2} \,.\, P_{CO}}{[1 + \alpha\, P_{CO} + \ (\beta P_{H_2})^{0.5}]^2}$	$\mathrm{K} = \mathrm{k}_4\mathrm{K}_2\mathrm{K}_3\mathrm{K}_4$ $\alpha = \frac{k_1}{k_{-1}}$	21.32

		$\beta = \frac{k_2}{k_{-2}}$	
FT-III-1	$-R_{CO} = \frac{K\,.\,P_{CO}}{1 + \alpha P_{CO}}$	$K = k_1$ $\alpha = \frac{k_1}{k_{-1}}$	29.36
FT-III-2	$-R_{CO} = \frac{K\,.\,P_{CO}P_{H_2}}{1 + \alpha P_{CO}}$	$K = k_2.K_1$ $\alpha = \frac{k_1}{k_{-1}}$	15.32
FT-III-3	$-R_{CO} = \frac{K\,.\,P_{CO}.P_{H_2}^2}{1 + \alpha P_{CO}}$	$K = k_3.K_1.K_2$ $\alpha = \frac{k_1}{k_{-1}}$	23.32
FT-IV-1	$-R_{CO} = \frac{K\,.\,P_{CO}}{1 + \alpha P_{CO} + \beta P_{H_2}}$	$K = k_1$ $\alpha = \frac{k_1}{k_{-1}}$ $\beta = \frac{k_2}{k_{-2}}$	18.30
FT-IV-2	$-R_{CO} = \frac{K\,.\,P_{H_2}}{1 + \alpha P_{CO} + \beta P_{H_2}}$	$K = k_2$ $\alpha = \frac{k_1}{k_{-1}}$ $\beta = \frac{k_2}{k_{-2}}$	28.65
FT-IV-3	$-R_{CO} = \frac{K.P_{CO}.P_{H_2}}{(1 + \alpha P_{CO} + \beta P_{H_2})^2}$	$K = k_3.K_1.K_2$ $\alpha = \frac{k_1}{k_{-1}}$ $\beta = \frac{k_2}{k_{-2}}$	32.12

Table 3

Parameter	Value	Dimension
E_a	105.00±3.70	kJ/mol
K_0	5.93×10^6	$mol.g_{cat}^{-1}.min^{-1}.bar^{-1}$
$k_{(573)}$	1.30×10^4	$mol.g_{cat}^{-1}.min^{-1}.bar^{-1}$
$k_{(583)}$	1.96×10^4	$mol.g_{cat}^{-1}.min^{-1}.bar^{-1}$
$k_{(593)}$	2.95×10^4	$mol.g_{cat}^{-1}.min^{-1}.bar^{-1}$
$k_{(603)}$	4.35×10^4	$mol.g_{cat}^{-1}.min^{-1}.bar^{-1}$
α_0	1.28×10^8	bar^{-1}
ΔH_{CO}	-68.00±4.50	kJ/mol
β_0	2.98×10^7	bar^{-1}
ΔH_{H2}	-48.00±3.20	kJ/mol
R^2	0.94	--
R^2_{adj}	0.91	--
R_{msd}	$3.9.18 \times 10^{-7}$	--
Variance	7.23×10^{-12}	--
MARR(%)	5.50	--

Table 4

NO	T (K)	Power low equation
1	573	$R_{573} = 9.13E^{-6} P_{CO}^{-0.27} P_{H_2}^{0.84} P_{H_2O}^{-0.23}$
2	583	$R_{583} = 1.44E^{-5} P_{CO}^{-0.18} P_{H_2}^{0.65} P_{H_2O}^{-0.15}$
3	593	$R_{593} = 2.23E^{-5} P_{CO}^{-0.09} P_{H_2}^{0.39} P_{H_2O}^{-0.11}$
4	603	$R_{603} = 2.38E^{-5} P_{CO}^{-0.08} P_{H_2}^{0.28} P_{H_2O}^{-0.08}$

Table 5

Parameter	Value	Dimension
E_a	95.54±2.5	kJ/mol
K_0	5.01×10^{3}	$mol.g_{cat}^{-1}.min^{-1}.bar^{-1}$
$k_{(573)}$	9.13×10^{-6}	$mol.g_{cat}^{-1}.min^{-1}.bar^{-1}$
$k_{(583)}$	1.44×10^{-5}	$mol.g_{cat}^{-1}.min^{-1}.bar^{-1}$
$k_{(593)}$	2.23×10^{-5}	$mol.g_{cat}^{-1}.min^{-1}.bar^{-1}$
$k_{(603)}$	2.38×10^{-5}	$mol.g_{cat}^{-1}.min^{-1}.bar^{-1}$
R^2	0.90	--
MARR (%)	8.86	--

Table 6